UNIVERSITY OF HELSINKI   REPORT SERIES IN PHYSICS

HU-P-D197

REACTION KINETIC MODELLING OF SIZE SELECTED GROWTH OF NANODOTS

Kirsi Riekki

Division of Materials Physics
Department of Physics
Faculty of Science
University of Helsinki
Helsinki, Finland

ACADEMIC DISSERTATION
To be presented, with the permission of the
Faculty of Science of the University of Helsinki, for public criticism
in Auditorium B123 of the Exactum, Gustaf Hällströmin katu 2b, on
November 23rd 2012 at 12 o'clock noon.

Helsinki 2012

Supervisor:

Dr. Ismo T. Koponen
Department of Physics
University of Helsinki
Helsinki, Finland

Pre-examiners:

Doc. Karoliina Honkala
Department of Physics, Nanoscience Center
University of Jyväskylä
Jyväskylä, Finland

Doc. Katariina Pussi
Department of Mathematics and Physics
Lappeenranta University of Technology
Lappeenranta, Finland

Opponent:

Prof. André Vantomme
Nuclear and Radiation Physics Section
Katholieke Universiteit Leuven
Heverlee, Belgium

Custos:

Prof. Kai Nordlund
Department of Physics
University of Helsinki
Helsinki, Finland

Preface

This thesis was done in Department of Physical Sciences at University of Helsinki and in former Laboratory of Physics at Helsinki University of Technology. I thank the head of the Department, Prof. Juhani Keinonen for providing me the working facility at University of Helsinki. I thank Prof. Tapio Ala-Nissilä for providing me an opportunity to do research in his research group in Helsinki University of Technology.

I wish to especially thank my excellent supervisor, Doc. Ismo T. Koponen. He has guided me throughout the long time of my graduate years with friendliness and patience, and his inspiration has encouraged me to complete this thesis. I also thank my custos, Prof. Kai Nordlund for all his valuable help in final preparation stage of the thesis and the defence. I would like to thank the pre-examiners of my thesis, Doc. Karoliina Honkala and Doc. Katariina Pussi, for careful reviewing of the manuscript.

I also wish to warmly thank my coauthor, Dr. Marko Rusanen, for his invaluable help during my early graduate study years. He, amongst other things, opened for me in detail the world of computational research of surface physics. I thank my coauthor, Dr. Kari Pirkkalainen for successful cooperation. For proofreading of the language of my thesis, I thank Janne Korpinen. My several roommates and members of research groups are acknowledged with thanks for discussions and help.

I thank Vilho, Yrjö ja Kalle Väisälä foundation for providing me the funding to finish my thesis.

Finally, the greatest thanks belong to my husband and children, and also for our parents for all the support during my graduate years 2004-2012.

Vantaa, October 2012

Kirsi Riekki

Abstract

The self-organized growth of nanodots and size selection are studied using reaction kinetic model rate equations. Two independent numerical methods and a mesoscopic continuous model are used to solve and analytically predict the details of the stationary nanodot size distribution.

The strongly reversible growth of kinetic origin is studied. The power-law distributions which are common in nature, display scaling of the size distribution with clearly defined scaling exponents. The stochastic simulation results and predictions of continuous model are in good agreement.

The self assembly of nanodots, observed in experiments and enabling the industrial use of dots in electronics, arises from the strain in heteroepitaxial growth systems and leads to uniform size distributions. To model the size selection, the size dependent thermodynamical energy of the nanodot is included into the reaction kinetics. The resulting distribution is studied in detail to resolve the overshooting phenomenon in which the mean of the distribution exceeds the thermodynamically favored size. The physical origin of the overshooting is explained as a combination of the reaction kinetics and the thermodynamical energy. The skewness of the size distribution is found from the numerical data, and it is added into the continuous model as a parameter to obtain an analytical estimate of the mean size.

The predictions of overshooting are calculated for two different types of growth; the 3D metal nanodots and semiconductor nanodots with double-well thermodynamical energy. The optimal, narrow size distributions are found, and external adatom flux from e.g. an external adatom source or ion beam assisted deposition improves the size selection by driving the size distribution to the narrowest location. Nucleation theory calculations of the thermodynamically stable distributions are performed, and the results are comparable to numerical and modelling results.

List of publications

This thesis consists of an introductory part followed by five research publications, which are cited by Roman numerals **I**–**V** in the text.

- Paper **I**: I.T.Koponen, and K.A. Riekki, Cluster growth poised on the edge of break-up: Size distributions, *Physica A* **387** (2008), 2504-2510.

- Paper **II**: K.A. Nevalainen, M. Rusanen, and I.T. Koponen, Size selected growth of nanodots: Effects of growth kinetics and energetics on the formation of stationary size distributions, *European Physical Journal B* **56** (2007), 311-322.

- Paper **III**: K. Pirkkalainen, K.A. Riekki, and I.T. Koponen, Two computational methods for describing size selected nanocluster growth and obtaining accurate cluster size distributions, *Computational materials Science* **43** (2008), 325-336.

- Paper **IV**: K.A. Riekki, Size selected growth of nanodots: Analytical prediction for the selected size, *European Physical Journal B* **85** (2012), 185.

- Paper **V**: K.A. Riekki, and I.T. Koponen, Size selected growth of nanodots: Ion beam assisted deposition and transition from 2D to 3D growth, *Nuclear Instruments and Methods in Physics Research B* **290** (2012), 48-53.

The author Kirsi Riekki née Nevalainen made the PCM simulations and data analysis of publications **I, II** and **III**, and has participated in writing the publications. The publications **IV** and **V** are based on the ideas developed during preparation of the Papers **I-III**. The author has done the analytical work and complete writing of the publication **IV**, and most part of the analytical work and complete writing of the publication **V**.

Papers **I**, **III** and **V** are reprinted by permission of Elsevier. Papers **II** and **IV** are reprinted by permission of Springer.

Symbols and abbreviations

BKL   Bortz-Kalos-Lebowitz algorithm
FPE   Fokker-Planck equation
IBAD   ion beam assisted deposition
MBE   molecular beam epitaxy
MED   master equation discretization
MMC   Metropolis Monte Carlo
PCM   particle coalescence method
RKM   reaction kinetic model

Contents

1

Introduction

The aggregates of small units are present in multiple contexts in nature, technological world and society. The general property of aggregates is that they are under constant change with respect to time; they grow and decay. The rates of their time development may depend e.g. on the size and the surroundings of the aggregate. The formation process is frequently self-organized; the growth of aggregates is directed by their internal properties. The aggregates can be micro- or nanometer scale particles, or, say, networks consisting of nodes. Some examples of microscopic scale particle growth are the formation of preplanetary and desert dust [1, 2, 3, 4]. More abstract examples are biological networks [5], cities and colonization [6] and scientific citation accumulation [7]. Some example of nanoscale aggregates are the metallic and semiconductor quantum dots [8, 9] which are the main research topic of this thesis.

The quantum dot is a mound of atoms which has a distinct lattice structure and two- or three-dimensional shape. The striking feature of quantum dots is that they show unique optical, electronical and magnetic properties in comparison with atoms, molecules and bulk materials. The phenomenon behind these properties is the quantum confinement; when the size of the quantum dot is similar to the Bohr radius (~ 10 nm) of its charge carrier exciton, the energy states are quantized [10, 11, 12]. Quantum dots have numerous technological applications within e.g. photonics, computer technology, medicine and biology.

Self assembly is an efficient technique to manufacture large amounts of dots with a sharp size distribution and adjustable mean size. The size of the quantum dot tunes the desired properties [13] and the size uniformity
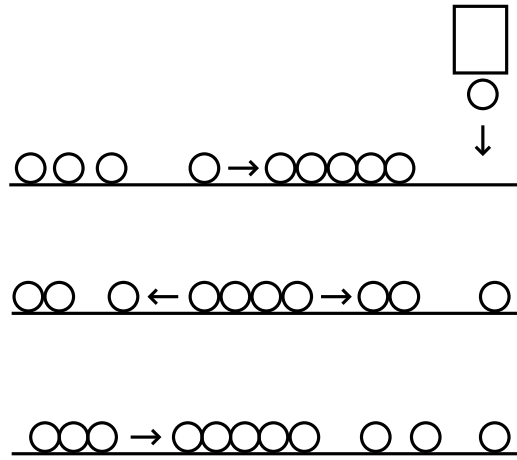
Figure 1.1: A schematic figure of growth processes at surface. Adatoms are deposited onto the surface. In principle, one nanodot can capture an adatom, or another nanodot of randomly selected size. Dot break-up is shown in the middle of the figure. The nanodots are surrounded by the adatom sea. In this work only adatom-dot processes are studied.

of dots is one of the main requirements for industrial-scale application use [14, 15]. Self assembly takes place e.g. during heteroepitaxial surface growth of quantum dots.

The surface growth begins with the deposition of adatoms to the surface using e.g. molecular beam epitaxy (MBE) [8, 16]. The deposition energies are typically thermal (~ 0.1 eV) in MBE and higher energies up to 30 eV in ion beam assisted deposition (IBAD) [17]. At the surface, the adatoms start to move randomly by thermal diffusion. After having an adequate amount of meandering adatoms (also called the adatom sea), one adatom attaches to another. Adatoms can attach to larger dots as well. Sometimes dots of randomly selected size can attach with each other. It is also possible to have one adatom detaching from a nanodot, or a nanodot fragmenting into two or more smaller dots or adatoms, as in hyperthermal deposition [17]. A schematic representation of the growth processes is shown in Figure 1.1.

In heteroepitaxial surface growth, the self-organization adjusts the size and distance of the dots. The elastic strain, arising from the lattice mismatch of substrate and the dot, forces the transition from a two-dimensional (2D) to three-dimensional (3D) dot, to lower the total energy. The thermodynamical

energy of dots is such that a minimum exists in the free energy difference, and size selection occurs as an interplay of the thermodynamical energy and the growth kinetics. The phenomena behind the size selection are to be clarified with theoretical studies connected with experimental observations.

The modelling of growth and stationary states of a quantum dot distribution consisting of hundreds of thousands of atoms is necessarily done by mesoscopic growth models instead of atomistic models. The structural details of quantum dots are excluded from these kinds of coarse-grained models, and the relevant parameters are the dot size, i.e. the number of atoms in dot, and the spatial dimension of the dot. The name "nanodot" describes the coarsened nature of quantum dots in the mesoscopic approach.

The growth model used in this thesis is a simplified, mesoscopic reaction kinetic rate equation model. The growth processes under consideration are adatom attachment, adatom detachment and deposition. The kinetical interaction strength, i.e. the transition rate of the nanodot is the edge length of a dot, determined by size and dimension [18, 19]. The phenomenological thermodynamical energy comprises the strain and the surface energy parts, and it is naturally incorporated into the transition rates of this model by a self-consistent scheme [20].

In a continuous mesoscopic model of the Fokker-Planck type, the time development of the nanodot distribution is presented in terms of the effective drift velocity and diffusion [21]. A Gaussian stationary nanodot size distribution is successfully predicted and the qualitative estimates for the selected size and the overshooting phenomenon in nanodot growth are obtained [21]. The overshooting means how much the distribution mean size exceeds the minimum of energy due to an interplay of kinetics and thermodynamical energy.

The phenomenological growth model is applied for different nanodot growth systems. In Chapter 2 the reversible kinetic power-law growth is studied. The scaling of the resulting distributions is researched. In Chapters 3-5, the thermodynamical energy is added, for the purpose of modelling self assembled, size selective growth. The resulting stationary Gaussian-type nanodot size distributions are studied. The goal is to clarify the overshooting phenomenon, firstly by stochastically simulating and using direct numerical integration scheme. Finally, an attempt to analytically estimate the amount of overshooting is made and the predictions are compared to numerical and experimental results [22, 23].

2

Kinetics of nanodot growth

In this chapter the kinetic nanodot growth in the presence of an adatom source is studied (Paper **I**). The size distribution of nanodots changes with the growing total nanodot mass, yielding power-law -type size distributions $n(s) \propto s^{-\tau}$. The distributions with small singularity exponents $0 < \tau \leq 1$ appear when attachment and detachment are both significantly affecting the forming nanodots, in other words the growth is strongly reversible. In nature one can see these kind of self-similar phenomena with power-law distribution [24, 25] with varying exponents τ in e.g. surface growth [17], preplanetary dust formation [1, 2], in mineral dusts over deserts [3, 4], and colonization [6].

2.1 Reaction Kinetic Model

The 2D surface nanodot growth is described with the Reaction Kinetic Model (RKM). In this simple model, only the reversible adatom exchange processes $A_1 + A_s \leftrightarrow A_{1+s}$ between a nanodot of size s and an adatom are taken into account. The rates of attachment and detachment are labeled by σ_s and γ_s, respectively. Their physical interpretation is that they are the probabilities at which the adatom is attached to or detached from a nanodot. The expressions are power-law dependencies of size with constant prefactors, $\sigma_s = \sigma_0 s^{\mu}$ and $\gamma_s = \gamma_0 s^{\alpha}$. In surface growth the rates are based on geometry; exponents μ and α are 1/2 for 2D nanodots, corresponding to the edge length of the nanodot ($\sigma_0 = \gamma_0 = 1$ assumed here). The continuous adatom flux Φ is deposited into system, guaranteeing the existence of an adatom sea. The

spatial correlations between nanodots are neglected, in consistence with an assumed dilute array of nanodots of size $s > 2$ (indeed, the density of adatoms at the surface is orders of magnitude larger than the nanodot density). Also the effect of spatial correlations into the rates is neglected, as well as the effect of atomic scale details at the nanodot edge.

The rate equations of number densities of adatom and cluster of size s (n_1 and n_s, respectively) are deduced directly from the adatom processes:

$$\frac{dn_1}{d\theta} = 1 - 2Rn_1^2 - Rn_1 \sum_{s \geq 2} \sigma_s n_s + \kappa R \gamma_s n_2 + \kappa R \sum_{s \geq 2} \gamma_s n_s; \qquad (2.1)$$

$$\frac{dn_s}{d\theta} = R\sigma_{s-1} n_{s-1} n_1 - R\sigma_s n_s n_1 + \kappa R \gamma_{s+1} n_{s+1} - \kappa R \gamma_s n_s \qquad (2.2)$$

where $\theta = \Phi t$ is the total mass, or coverage of the system and $R = \sigma_0/\Phi$ and $\kappa = \gamma_0/\sigma_0$ describe the relative strength of deposition and detachment to attachment. The model is directly comparable to the model used in scaling theory [26, 27].

The results show three different cases of growth [26, 27, 28]. Firstly, there is the attachment-dominated case, when $\mu > \alpha$ and no stable solutions are found. Secondly, when $\alpha > \mu$, the detachment dominates and the growth is stagnated. The third and most interesting case occurs when the exponents are equal in value and $0 < \mu = \alpha \leq 1$. In this symmetric case a steady state solution can be found, and scaling properties are expected [29, 30].

In steady state of growth the nanodot distribution is stationary, $dn/dt = 0$. It is now possible to obtain from equation (2.1) a condition for stationary adatom density $n_1 \to \kappa$. Setting $n_1 = \kappa$ and redefining $\theta \to \theta \kappa R$, the nanodot density (2.2) simplifies to a general, discrete growth equation, also known as the Becker-Döring equation [31, 32]:

$$\frac{dn_s}{dt} = \sigma_{s-1} n_{s-1} - (\sigma_s + \gamma_s) n_s + \gamma_{s+1} n_{s+1} \qquad (2.3)$$

and with equal growth exponents $\mu = \alpha$ the equation is

$$\frac{dn_s}{dt} = (s-1)^\alpha n_{s-1} - 2s^\alpha n_s + (s+1)^\alpha n_{s+1}. \qquad (2.4)$$

At the continuum limit of size $s \to x$, one finds the scaling function for the distribution $f(x)$ and the dynamic scaling properties, including the dynamic growth exponents of mean size and nanodot density. The continuous model of power-law growth is introduced in the next section.

2.2 Continuous model

In this section a continuous model is derived from the discrete reaction kinetic model (2.4). The size variable s is changed into a continuous variable x, having values $x \geq 1$. The next step is to determine the moments of the size distribution [33] from equation (2.4). The first two moments $m_{1,2}$ are calculated from attachment and detachment rates directly:

$$m_i(x, \theta) = \frac{1}{i!} \left[\sigma_x + (-1)^i \gamma_x \right], \ i = 1,2 \tag{2.5}$$

giving $m_1 = 0$ and $m_2 = x^\alpha$. The continuous differential equation for distribution, the Fokker-Planck equation (FPE), is obtained as a truncated Taylor-type series of moments [33]:

$$\frac{\partial n(x, \theta)}{\partial \theta} = \sum_{i=1}^{2} \left(\frac{\partial}{\partial x} \right)^i (-1)^i \left[m_i(x, \theta) n(x, \theta) \right] \tag{2.6}$$

$$\Rightarrow \frac{\partial n(x, \theta)}{\partial \theta} = \frac{\partial^2}{\partial x^2} \left[x^\alpha n(x, \theta) \right]. \tag{2.7}$$

This is a non-linear diffusion equation with solution presented in reference [34]:

$$n(x, \theta) \propto x^{-\alpha} \exp \left[-\frac{x^{2-\alpha}}{(2-\alpha)^2 \, \theta} \right], \tag{2.8}$$

When $\alpha \leq 1$ the result is a singular power-law distribution with an exponentially decaying stretched tail. The solution of equation (2.8) gives the scaling property $x \to x/\theta^\beta$, with the dynamic growth exponent

$$\beta = 1/(2 - \alpha). \tag{2.9}$$

The FPE usually contains only the two first terms of the series expansion, although the series (2.6) should include an infinite number of terms. Due to this truncation, there is no guarantee of convergence in cases where the higher moments $m_{i \geq 3}$ are nonzero, as in the current case. However, it turns out *a posteriori* that the continuous growth equation produces a good description of the reaction kinetic model (2.2).

2.3 Computational approach: Particle Coalescence Method PCM

The time developments of rate equations are solved numerically using the revised Particle Coalescence Method PCM [29, 30] which is a stochastic Metropolis Monte Carlo (MMC) simulation [35, 36, 37, 38]. In a typical surface growth situation, the time scale is varying; the shortest time scale of $\sim 10^{-13}$ seconds is connected to the diffusive adatom jumps at the surface, and the longest time scales of order of second are connected to the dot shape transitions [8]. Simulation of systems having such huge, varying time scales is a demanding task and becomes unfeasible with deterministic simulation schemes like Molecular Dynamics simulation, but instead the stochastic MMC simulation method is applicable.

In MMC simulation, the simulated next state only depends on the present state as a Markov chain. The possible events are, in current case of adatom processes only, the attachment, detachment and deposition, with total rates $\Gamma_{att}, \Gamma_{det}$ and Γ_{dep}, respectively. The rates of all possible events must be known in advance, and kept updated during the whole simulation. The dot sampling is done one event at a time, firstly choosing the final state f with uniform probability $1/N$, where N is the total amount of possible events. The final state is accepted as a new state with probability $\nu_{i\to f}/\nu_{max}$, where $\nu_{i\to f}$ is the transition rate between initial state i and final state f. The maximum of all transition rates is ν_{max} and the total transition rate Γ_c is given by $\Gamma_c = N\nu_{max} = \Gamma_{att} + \Gamma_{det} + \Gamma_{dep}$ for a certain dot configuration c. Configuration c is a list of dots, where each dot has a size label of integer number. In typical simulation of power-law growth, approximately 60000 adatoms are deposited, corresponding to the coverage $\theta = 0.25$ of the simulation lattice having $L^2 = 500^2$ lattice sites. The conservation of mass is ensured by keeping the number of dots smaller than the maximum amount of lattice sites.

The time step corresponding to the event is drawn stochastically from the Poisson distribution: $\Delta t = -\ln(u)/\Gamma_c$, where u is random number $0 \leq u \leq 1$. Due to the stochastic nature of the time step determination, the error of simulation time arises and the time-dependent observables have to be calculated by averaging. In MMC simulations, the averaged simulated time step is realistic, when realistic transition rates are inserted.

The dots are assumed point-like and the dot-adatom event probabilities are established in terms of attachment and detachment rates. The dots are

labeled by their size and randomly positioned in an artificial simulation lattice, with no connection to physical lattices. The point-like island assumption corresponds to a mean-field approximation and holds at low coverages. Consequently all geometrical details of transition rates and correlations between dots are neglected.

In mean-field approximation, the mixing of dots has to be taken care of, in addition to the diluteness. The mixing could be done by allowing the dots to jump between simulation lattice sites to find adatom (adatoms are taken into account as dots of size 1) for attachment, but it is a heavy computational task. The problem is bypassed by removing the jumps and finding merely the probability for attachment event between two dots. The detachment and deposition rates need to be corrected with the factor depending on the empty lattice sites $L^2 - N_{dots}$, where L is the size of the lattice and N_{dots} is the number of dots. The total rates are [29, 30]

$$
\begin{aligned}
\Gamma_{att} &= \nu_{max}^{att} N_{ada}(N_{dots} - 1); \\
\Gamma_{det} &= \nu_{max}^{det}(N_{dots} - N_{ada})(L^2 - N_{dots}); \\
\Gamma_{dep} &= L^2 \Phi(L^2 - N_{dots});
\end{aligned}
\tag{2.10}
$$

where ν_{max} is a maximum transition rate of attachment and detachment, Φ is the deposition flux and N_{ada} is the amount of adatoms which is also included into N_{dots}.

2.4   Results of power-law growth

The symmetric cases $\alpha = \mu$ were simulated with $\alpha = 0, 1/4, 1/2, 3/4$ and 1, as well as some cases where $\alpha > \mu$ and $\alpha < \mu$. Values of the parameters κ and R were chosen to obtain the scaling region. For clarity, the ratio of detached atoms to deposited atoms $N_{det}/N_{dep} = 10^{-2}\kappa R$ is defined (for details, see Paper **I**) and the values of κ and R were chosen to give $0.1 < N_{det}/N_{dep} < 10^4$. The region $N_{det}/N_{dep} > 1$ was of particular interest.

2.4.1   Dynamical growth exponents

In PCM simulations, a power-law scaling behaviour for distribution mean size $\langle s \rangle$ and total nanodot density N is found. A well-defined scaling exponent β as a function of time is found for $\langle s \rangle$ and exponent $1 - \beta$ for N with
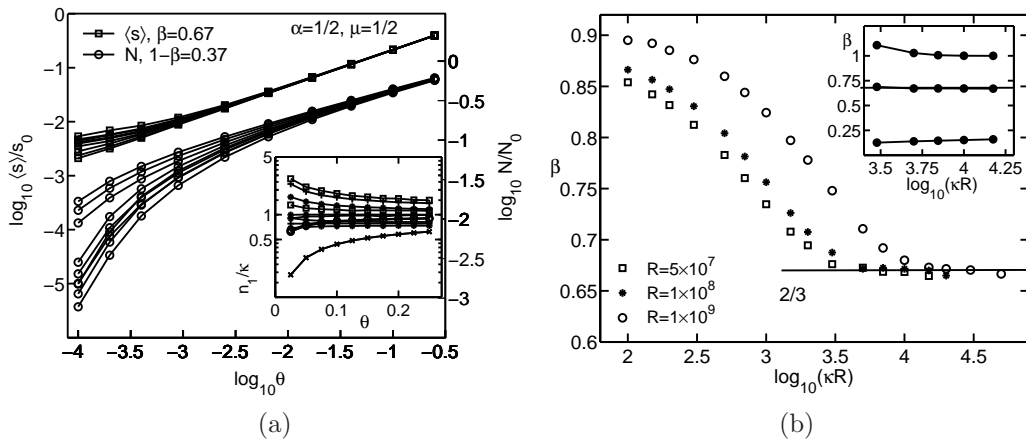
Figure 2.1: a): The mean size of nanodots $\langle s \rangle$ ($\square$) and the total nanodot density N ($\bigcirc$) for the symmetric case with $\alpha = \mu = 1/2$ as a function of the filling fraction θ. In the inset is shown the scaled monomer density n_1/κ for cases $N_{det}/N_{dep} = 1$ ($\square$), 10 (+), 10^2 (*), 10^3 ($\bigcirc$), and 10^4 ($\times$) from top to bottom. Figure b): The dynamic exponent β for the symmetric case $\alpha = \mu = 1/2$ as a function of κR demonstrating the transition to the growth regime with analytical prediction of β given by equation (2.9) (the horizontal line). For comparison, the inset shows additional results for β in the asymmetric cases with $\alpha = 1/2$ and values $\mu = 1, 1/2$ and 0, from top to bottom.

$\alpha = \mu = 1/2$. The simulation results are presented in figure 2.1a and the values of exponents agree with the scaling theory results [26]. In addition, in figure 2.1a the scaled adatom density n_1/κ as a function of total coverage θ is shown. One can see, that the simulation results confirm the assumption $n_1 \to \kappa$ made in deriving the continuous growth equation in Section 2.1.

The dynamic exponent β is a good indication of the growth regime of the distribution. The figure 2.1b shows the behaviour of exponent β as a function of product κR. At small κR, the detachment is negligible to attachment, and the growth is irreversible [29, 30], and the growth exponent $\beta \approx 1$ is not constant in time. The transition of growth mode at large κR is clearly seen. In that case detachment is comparable to attachment and the system is reversible. The scaling is observed and the analytical model of Section 2.2 is applicable.

The other symmetric cases $\alpha = \mu = 0, 1/4, 3/4$ and 1 were simulated

Table I: The dynamic scaling exponent β, the exponent τ and the constant x_0 of the scaling function $f(x) \propto x^{-\tau} \exp[-x/x_0]$ from the PCM simulations for the symmetric case $\alpha = \mu$. In all values the statistical error of simulations is 0.01 or smaller.

α	0	1/4	1/2	3/4	1
β	0.50	0.57	0.67	0.80	0.99
τ	0.06	0.29	0.54	0.77	1.01
x_0	5.35	5.26	7.34	5.04	3.16

and the results of growth exponent β are in good agreement with analytical predictions (see Table I).

2.4.2 Scaling function of island distribution

The distribution has, according to PCM simulations, a form of exponential $f(x) \propto x^{-\tau} \exp[-x/x_0]$ at the scaling regime of large detachment $N_{det}/N_{dep} \gg 1$. The scaled distributions with $\alpha = \mu = 0, 1/2$ and 1 are presented in figure 2.2. The power-law leading edge of distribution emerges already at $N_{det}/N_{dep} \approx 1$, but completes only at $N_{det}/N_{dep} \approx 100$, as is shown in the inset of figure 2.2.

The fitted values τ, shown in Table I, are close to the analytical prediction $\tau = \alpha$, when $0 \leq \alpha \leq 1$ (Section 2.2). However, the values of τ are systematically larger.

The theoretical prediction for the distribution from the continuous Fokker-Planck equation is a streched exponential function, equation (2.8). On the other hand, the simulations indicate that the distribution is exponential without stretching. This discrepancy is probably resulting from the stochastic nature of PCM simulations compared to the deterministic continuum model.

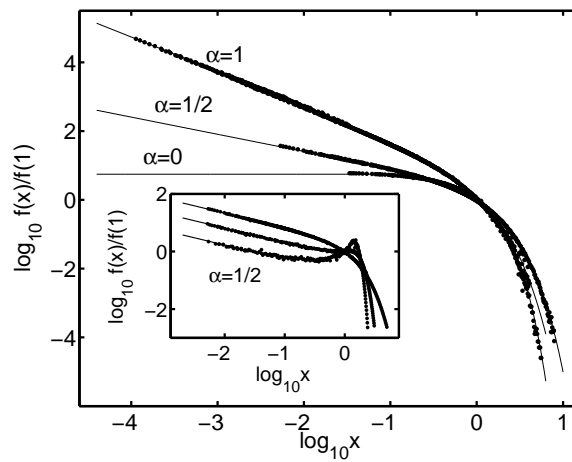Figure 2.2: The scaling function $f(x)/f(1)$ for the symmetric case with $\alpha = \mu = 0$, 1/2, and 1. The fitting function (given in the text) with τ and x_0 as in Table I is shown with the solid line. In the inset the scaled size distributions are shown with $\mu = \alpha = 1/2$ at $N_{det}/N_{dep} = 1$, 10, and 10^2 from bottom to top. The solid lines in the inset correspond to the power law $x^{-1/2}$.

3

Size selection growth model

The self assembly is observed experimentally in two modes of surface growth. The first mode is the Stranski-Krastanov growth [39], with nanodots nucleating in a wetting layer of adatoms covering the substrate. The other strained growth mode is the Volmer-Weber growth [40, 41, 42], in which the nanodots nucleate directly at the substrate without a wetting layer. The self assembly is mostly seen in heteroepitaxial semiconductor materials, but it occurs also in heteroepitaxial metals [39, 42, 43, 44, 45].

In self assembly of nanodots, the interesting feature is the size selective growth of nanodots [39, 40, 41, 42, 46, 47]. The thermodynamical energy of strained heteroepitaxially growing structures arises from the difference of lattice constants of substrate and the deposited material. The total energy of a nanodot is a combination of the surface energy and the elastic strain relaxation energy contributions. An important characteristic of the thermodynamical energy is, that a minimum of free energy difference exists [48, 49, 50, 51]. The thermodynamically controlled growth results in a stable equilibrium distribution of Gibbs-Boltzmann type, where the favored size is determined by the total energy minimum [52, 53, 54, 55]. The physical origin of spontaneous size selection is the interplay of the growth kinetics and the thermodynamical energy.

In this chapter, the reaction kinetic model for size selective growth is obtained from the power-law growth model by including the thermodynamical energy. This model is a general mesoscopic model with phenomenological level properties. For example, the strain energy is taken into account, but the wetting layer, although present at the experimental Stranski-Krastanov growth situation, is not explicitly included into the growth model. Therefore

the same model can be applied for different types of nanodot growth systems by only choosing the relevant growth exponents and parameters for phenomenological energy, although more realistic energy functions can certainly be included for specific systems. The basic equations behind the continuous model of size selection are the reaction kinetic equations, already presented in Chapter 2 in equations (2.1)–(2.2). Papers **II**–**V** are based on this model.

3.1 Self-consistent reaction rates

The simple power-law growth model presented in Chapter 2 does not include the free energy difference of growing islands. The thermodynamical energy is incorporated into the transition rates by the self-consistent reaction rate scheme presented in reference [20]. In the self-consistent scheme, the adatom density is calculated at the dot boundary with two assumptions. Firstly, the "bare" adatom detachment rate from the edge of the dot of size s is different from the effective escape rate γ_s, at which the adatom leaves the capture zone of dot and ends up in the adatom sea. Secondly, the effective rate γ_s depends on the concentration of adatoms on the dot edge, and the rate is modified by the energy barrier Δ_s to include the re-adsorption of adatoms. (The form of energy Δ_s is specified later.) The self-consistent rates σ_s and γ_s are too complicated for the purpose of this model. With simplifying details (see Appendix A of Paper **II**), the simple form of rates is obtained:

$$\begin{aligned}
\sigma_s &= s^q/(\xi + e^{\beta \Delta_s}) \\
\gamma_s &= s^q/(1 + \xi e^{-\beta \Delta_{s-1}}).
\end{aligned} \tag{3.1}$$

The detachment rate γ_s is shown in figure 3.1 for three temperatures. The parameter ξ is the correlation length, i.e. the average length that adatoms travel before they are captured, and it is a free parameter in RKM, defining the density of the dots. In this work it has the value $\xi = 0.01$. In Papers **II** and **III** the reaction rates are erroneous; the corrections are found in Appendices A and B of this thesis. The rates fulfill the requirement of detailed balance, arising from reversibility:

$$\frac{\gamma_{s+1}}{\sigma_s} = e^{\beta \Delta_s}. \tag{3.2}$$

However, the attachment rate σ_s in equation (3.1) has very low values at small sizes, thus unnecessarily slowing down the first steps of the growth.
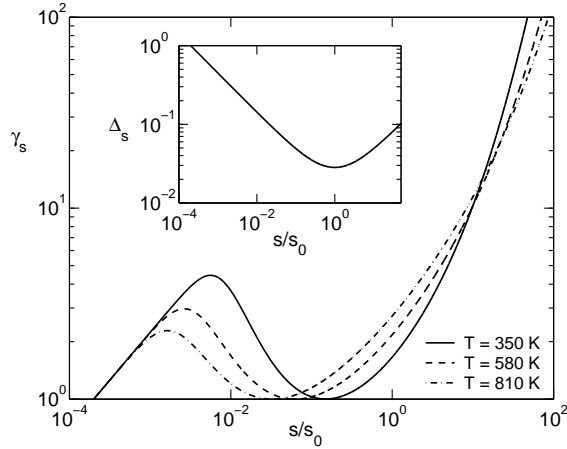
Figure 3.1: The detachment rates γ_s as a function of dot size s/s_0 at three different temperatures $\beta^{-1} = 0.03, 0.05$ and 0.07, corresponding to $T = 350$, 580 and 810 K. The thermodynamical energy function Δ_s is specified in equation (3.3) and parameters are $c = 0.0002$ and $\alpha = 0.5$. The minima of rates are at sizes $0.15s_0$, $0.06s_0$ and $0.03s_0$, where $s_0 = 5000$. In the inset is the free energy difference Δ_s which has minimum at s_0.

From figure 3.1 is cleary seen as a saddle point, a critical size, over which the distribution has to travel in order to show the effect of the thermodynamical energy. Below saddle point, the deposition defines the time scales of the growth. The attachment rate can thus be approximated

$$\sigma_s \to s^q$$

to fasten the growth towards the critical size. The initial stage of growth is essentially the reversible power-law case described in Chapter 2.

3.2   Free energy difference

The essential feature of nanodot growth energy is the *free energy difference* Δ_s for a dot of size s. The free energy difference is described by total free energy E_s per atom of the nanodot of size s: $\Delta_s = E_{s+1} - E_s$. In this work, we use a simple, phenomenological form of total free energy introduced by Gai et al. [42]. There are, however, several other energy functions available, but

they are either more complicated [43] or they do not correctly reproduce the thermodynamical energy of metallic nanodots [56, 57]. The simple expression for free energy difference is [42]

$$\Delta_s = w_0 + cs^\alpha + as^{-p} \tag{3.3}$$

where the second term is the contribution of self energy and the third term is the surface energy of the dot. The self energy includes strain energy, interface energy and step energy. The last term with $a = g\theta^{2/3}$ describes the contributions of coverage dependent dot-dot interactions with coupling strength g, and possibly also the contribution of the Gibbs-Thomson effect [56, 58]. The parameter w_0 is the constant part of self energy, which sets the minimum value of the total free energy.

To reduce the amount of free parameters, the redefinition $a \to 1$ is made, giving the minimum of thermodynamical energy at $s_0 = a/c \to 1/c$ and scaling $\beta \to a\beta$, $c \to c/a$ and $w_0 \to w_0/a$. The parameter α is proportional to the nanodot substrate geometry and describes the strength of the edge energy to the surface energy.[1] In this work, the equation (3.3) is used as a flexible fitting formula for several types of energy functions of different physical origin.

The free energy difference Δ_s in (3.3) actually is the energy needed to attach or detach one adatom of dot of size s. At continuum limit the free energy difference corresponds to chemical potential $\mu(s) = \partial E(s)/\partial s$. With parameter choice used in Paper **II**, $c = 0.0002$, the minimum location is $s_0 = 5000$. The parameter $w_0 = -0.2783$ adjusts the depth of the minimum, chosen to give $\Delta(s_0) = -0.25$ (see inset of figure 3.1) to obtain convenient depth for numerical simulations.

3.3 Continuous model

The continuous growth model is derived from two basic assumptions. Firstly, the detailed balance condition in terms of the transition rates σ_s and γ_s is

$$\sigma_s n_s^{eq} = \gamma_{s+1} n_{s+1}^{eq}. \tag{3.4}$$

---

[1]The energy parameter α is now different from the power of detachment rate s^α. The kinetic rate exponent is called q from this on, corresponding to attachment rate σ^q and detachment rate γ^q.

Secondly, the equilibrium size distribution n^{eq} is assumed to be the Gibbs-Boltzmann distribution

$$n_s^{eq} = \exp\left[(s\bar{\Delta} - E_s)/k_B T\right] \tag{3.5}$$

where $\bar{\Delta}$ is the *average chemical potential* of the dot distribution and E_s is the total internal energy of a dot of size s.

A net mass flux $J(s,t)$ occurs between dots of sizes s and $s+1$: [21, 32]

$$J(s,t) = \sigma_s n_s(t) - \gamma_{s+1} n_{s+1}(t) \tag{3.6}$$

where t is time and n_s and n_{s+1} are the non-equilibrium distributions. The size variable $s \to x = s/s_0$, attachment rate $\sigma_s \to \sigma_x = x^q$ and size distribution $n_s \to n_x = n$ are taken to the continuum limit to obtain [21, 32]

$$J(x,t) = x^q \left[\frac{\bar{\Delta} - \Delta}{k_B T} n(t) - \frac{\partial n(t)}{\partial x}\right] \tag{3.7}$$

where the equilibrium distribution (3.5) is given in terms of the chemical potential, now defined as $\Delta = \partial E/\partial x$.

The continuity equation is

$$\frac{\partial n(t)}{\partial t} = -\frac{\partial J(x,t)}{\partial x}. \tag{3.8}$$

From this expression one obtains the continuous growth equation, also known as the Fokker-Planck equation:

$$\frac{\partial n(t)}{\partial t} = -\frac{\partial}{\partial x} v_{eff}(x,t) n(t) + \frac{\partial}{\partial x}\left[x^q \frac{\partial n(t)}{\partial x}\right]. \tag{3.9}$$

The first term of the right-hand side is the drift contribution with *drift velocity* given by

$$v_{eff}(x) = x^q(\bar{\Delta} - \Delta)/k_B T. \tag{3.10}$$

The drift velocity describes the deterministic effect of chemical potential difference $\bar{\Delta} - \Delta$ on dot growth. The last term in equation (3.9) is the diffusion contribution.

3.4 Computational approach

The numerical results of the size selective RKM are calculated independently using the PCM simulation method with the efficient Bortz-Kalos-Lebowitz algorithm (Paper **II**) and by direct numerical integration of rate equations (Paper **III**). The properties of these numerical methods are explained below.

16

3.4.1 Bortz-Kalos-Lebowitz algorithm

The Metropolis Monte Carlo MMC based computational scheme, the revised Particle Coalescent Method PCM described in Sec. 2.3 is used to simulate the solution of the rate equations (2.1)–(2.2) with respect to time. The thermodynamical energy is now included into the growth model, and the existence of a minimum in energy slows down the distribution significantly and the revised PCM simulation cannot be used. A more efficient algorithm is needed.

The study of the stationary state is possible when the trial-based MMC algorithm is changed into the rejection-free Bortz-Kalos-Lebowitz (BKL) algorithm [59] also known as the Kinetic Monte Carlo algorithm [60, 61]. In the BKL algorithm, at each time step some event is chosen with correct statistical weight according to the probabilities, leaving no rejected attemps. In order to choose the weight of the event correctly, the total rate Γ_c is needed at each time step for the dot configuration c. Typical dot configuration of size selective growth includes approximately 120000 adatoms, corresponding to the coverage $\theta = 0.5$ of the simulation lattice (500^2 lattice sites). One possible option for the storage of transition rates is the binary tree structure, although its implementation is a demanding task [62]. The searching of the binary tree is efficient, but the updating is somewhat more complicated. The length of the time step is drawn as in Sec. 2.3.

3.4.2 Master Equation Discretization

The Master Equation Discretization (MED) scheme is a direct numerical integration of the reaction kinetic model, and also recommendable for solving the corresponding continuous growth equations [63]. The derivation of the discretized equation of RKM begins with the Becker–Döring equation (2.3) which is written in terms of discrete differential operator $D[u_k] = u_k - u_{k-1}$ as

$$\frac{dn_s}{dt} = D[D(\kappa\gamma_{s+1}n_{s+1})] - D[(n_1\sigma_s - \gamma_s)n_s]. \tag{3.11}$$

At the limit of small variations ($\kappa_{s+1} \approx \kappa_s; n_{s+1} \approx n_s$) the Fokker-Planck equation of growth is accomplished with time dependent drift and velocity coefficients [64] (see also equation (3.9)). The equivalence of discretized RKM and the continuous model is explicitly shown. According to reference [63] this

equation can be expressed in linear and centered discretization form:

$$\frac{dn_s}{dt} = \epsilon^{-2}\{n_{s-1}[D_0 + (\phi_s - \phi_{s-2})/4] - n_s[2D_0] + n_{s+1}[D_0 - (\phi_{s+2} - \phi_s)/4]\}$$
(3.12)

where ϵ defines the discretization lattice size and the potential ϕ is the drift velocity field. The difficulty in numerics with the discretized equation (3.12) appears at the next nearest neighbour terms $s \pm 2$ connected to the curvature of the drift velocity field. By a mathematical transformation the equation (3.12) is written in the corresponding form of

$$\begin{aligned}
\frac{dn_s}{dt} &= D_0\epsilon^{-2}\{n_{s-1}\mathrm{e}^{-(\phi_s-\phi_{s-1})/D_0} - n_s[\mathrm{e}^{-(\phi_s-\phi_{s+1})/D_0} + \mathrm{e}^{-(\phi_s-\phi_{s-1})/D_0}] \\
&\quad + n_{s+1}\mathrm{e}^{-(\phi_{s+1}-\phi_s)/D_0}\}.
\end{aligned}$$
(3.13)

This equation is directly equal to the discrete Becker–Döring growth equation (2.3). To show the complete equivalence of MED and RKM, the drift velocity field is connected to the thermodynamical energy of growth by defining $(\phi_{s+1} - \phi_s)/D_0 \equiv \beta\Delta_s$. The curvature of the velocity field is now incorporated into the exponential terms of only nearest neighbours $s \pm 1$, and the numerical solution is feasible.

The two solution schemes, PCM and MED, are thus independent and shown to be equivalent with the continuous growth model at the stationary region of growth.

4

Results: distribution

The two numerical schemes, PCM simulations and numerical integration of the RKM are used to calculate the time development of the size distributions. Very similar results are obtained with both of the solution methods in every aspect of the study, implying that the solution is the correct one and that the phenomenological behaviour of the solution of the growth model is attained from the numerical results.

The results show that there are three distinct stages of growth. Firstly, there is the singular, scaling-law-type distribution at early stages of growth. Secondly, the kinetically determined, short-lived metastable state is found at the minimum of the detachment rate (see figure 3.1). Thirdly, there is the stationary state which occurs when the distribution mean has exceeded the location of the free energy difference minimum.

4.1   Initial stage

The initial development of the distribution begins with the deposition of adatoms and proceeds to small nanodot sizes. At low temperatures the thermodynamical energy in the detachment rate does not affect the growth at small sizes (figure 3.1), leaving only the kinetic contribution s^q into the rates (Section 3.1). The growth is reversible and in principle comparable to the power-law growth in Chapter 2.

The simulations show that the nanodot distribution at the initial stage is some kind of singular distribution with a large density of small islands. The scaled initial size distribution $f(x)/f(1)$ is shown in figure 4.1 with two
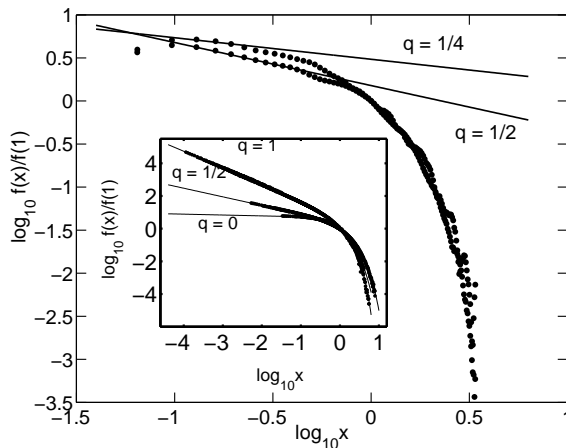
Figure 4.1: The scaled initial singular distribution $f(x)/f(1)$ as a function of scaled size x. Figure contains data sets with two different values for the kinetic exponent q (at $T = 70K$, $c = 0.0002$ and energy parameter $\alpha = 1/2$). The inset shows the reversible growth results from longer simulations presented in Chapter 2. The error bars are smaller than the symbol sizes.

kinetic exponents q. In the inset are shown the distributions from power-law growth for comparison. One sees similar shapes of distributions with singularity s^{-q}, and the approximate dependence of exponent q. The region of scaling is very narrow (below the critical size in detachment rate, figure 3.1), and the scaling exponents cannot be reproduced accurately from the initial stage data. However, the simulations confirm that the results of initial growth stage resemble the results of singular power-law growth.

4.2   Intermediate metastable state

When the nanodot distribution has exceeded the critical size in the detachment rate, the deposition is turned off and the distribution continues to develop only driven by the reaction kinetics. At the same time, the initial power-law type distribution transforms into a propagating Gaussian-type distribution with disappearing singularity at small sizes (figure 4.2a). Eventually only the somewhat Gaussian-type part of the distribution, going towards larger sizes, is left. The distribution finds a seemingly stationary state well
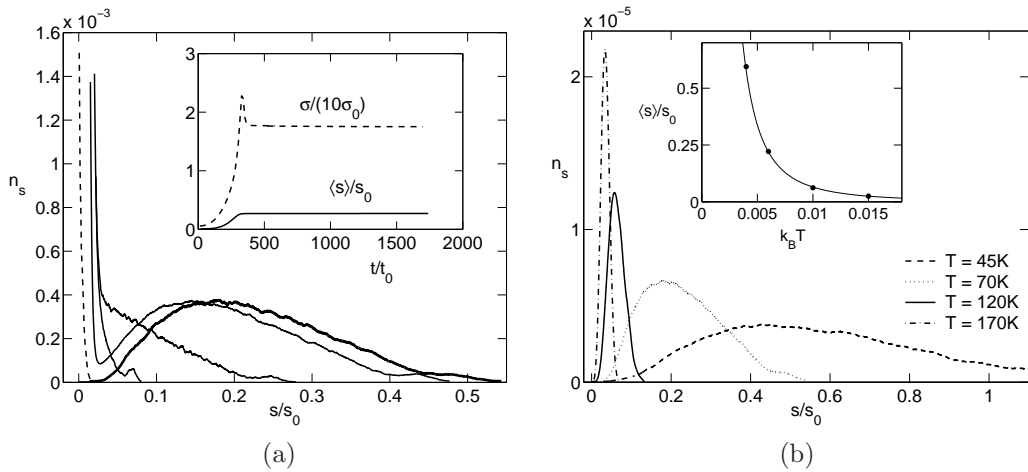
Figure 4.2: a): The size distribution n_s as a function of size s/s_0 in the intermediate stationary stage of growth. The stationary state is determined by the minimum of the detachment rate, which occurs with current parameters at $0.27s_0$. The mean and standard deviation of the distribution are shown in the inset. Figure b): The stationary size distributions n_s at different temperatures in the intermediate stationary stage of growth. The inset shows the temperature dependence of mean size $\langle s \rangle / s_0$ of the distributions (dots) and the fit. In both figures the distributions are multiplied for clarity. Parameters are $T = 70$ K, $\alpha = q = 0.5$, $\kappa = 10^{-7}$, $c = 0.0002$, $\sigma_0 \approx 30$, and $t_0 \approx 10$.

below the free energy minimum, namely at the location of the detachment rate minimum. The distribution mean size and standard deviation take a constant value, as shown in the inset of figure 4.2a. Actually, this state of the distribution is a short-lived metastable state, originating from the reaction kinetics and controlled by the energy parameter w_0. The simulated properties of intermediate metastable state correspond well to experimental results of kinetically controlled stationary states [48].

In experimental nanodot systems, the metastable state may be a long-term state in realistic time, depending on the parameters of the real thermodynamical energy. Also in trial-based MMC simulations, it is possible for the distribution to stay practically forever in the intermediate metastable state. The event-based BKL-algorithm, used in this study has a clear advantage in simulating long-lived metastable states. Using BKL, the distribution simply

continues to develop further on from the intermediate state with reasonable computing times.

Temperature affects the distribution at the intermediate state remarkably (figure 4.2b). The dependence of the mean size and temperature is roughly inverse power-law type $\langle s \rangle \propto (k_B T)^{-k}$ with $2 \lesssim k \lesssim 3$ (for details, see figure 6 in Paper **II**). The origin of the strong effect is in the existence of the free energy difference; thermally activated adatom processes are weighted differently with a geometric factor s^q.

Finally, after leaving the intermediate metastable state, the distribution takes the stationary form which occurs above the free energy difference minimum. The results of the stationary distribution are presented in the next Chapter.

4.3   Stationary size distribution

The stationary state is found when the distribution exceeds the free energy difference minimum (see figure 4.3a). The mean size of islands $\bar{x} = \langle s \rangle / s_0$ and the standard deviation of distribution σ stabilize, and the island distribution takes a nearly perfect Gaussian form (Fig 4.3b). The time development of the distribution is extremely slow, and the shape of the distribution is maintained. The striking feature of the stationary distribution is that the mean size of the island distribution systematically overshoots the free energy minimum location. This is also seen in the work by Jesson et al. [21]. In addition, a minor but important skewness remains in the size distribution, as is found in Papers **II** and **III**. In this chapter a continuous model, derived from the discrete growth equations, is used to predict mean, standard deviation and drift velocity of the distribution.

4.3.1   Time evolution of mean and width

The distribution mean and standard deviation have a clear time development before they stabilize into constant values of the stationary state. The time evolution of the size distribution is obtained from the growth equation using a pure Gaussian distribution with time dependent mean $\bar{x}(t)$ and variance $\sigma^2(t)$. In principle the mean and variance are obtained by integral transformations of growth equation [65, 66], but a more convenient choice is to use differential equations [67]. The distribution is assumed narrow enough for
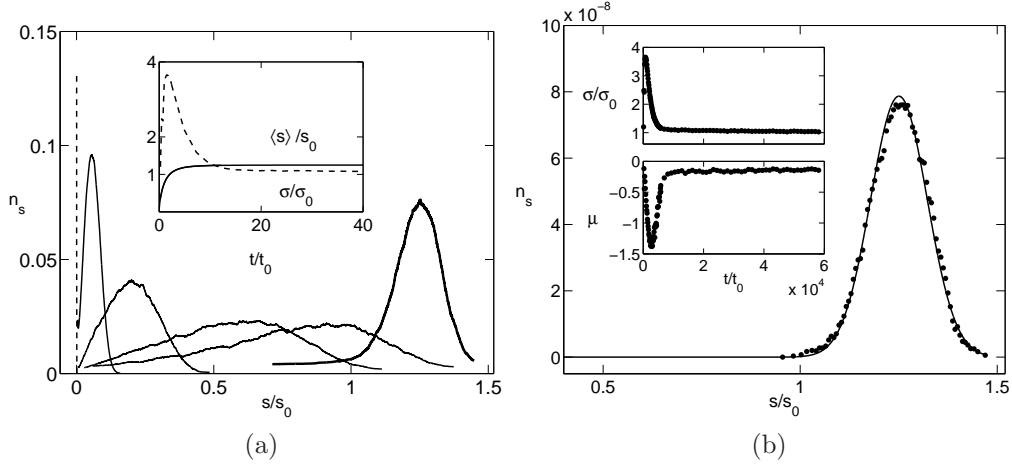
Figure 4.3: a): The time development of size distributions n_s as a function of size s/s_0. The initial singular distribution is marked with a dashed line. For clarity, the other distributions are multiplied (factors in Paper **II**). In the inset are shown the average dot size $\langle s \rangle /s_0$ (solid line), and the standard deviation of the distribution σ/σ_0 (dashed line). The stationary width is $\sigma_0 \approx 350$. Figure b): The stationary size distribution n_s at the final metastable state ($t = 1.0 \times 10^8, \kappa = 1.0 \times 10^{-7}$, $c = 0.0002$, $\alpha = 0.5$ and $T = 350$K). PCM simulations are marked with dots and the Gaussian distribution with a solid line. Note the skewness of distribution compared to the Gaussian. In the upper inset the time development of the standard deviation σ/σ_0 and in the lower inset the skewness μ are shown. The parameter $t_0 \approx 1.7 \times 10^3$.

chemical potential linearization, which also enables the linear drift velocity of the mean size, giving

$$\frac{d\bar{x}}{dt} = \beta D(\bar{\Delta} - \Delta) - \beta D \Delta'(\bar{x} - x_0), \qquad (4.1)$$

$$\frac{d\sigma^2}{dt} = 2D - 2\beta D \Delta' \sigma^2. \qquad (4.2)$$

The time evolution of mean size, standard deviation and skewness are similar in stochastic PCM simulation (Paper **II**) and in direct numerical integration of RKM (Paper **III**).

After redefinitions, one obtains differential equations for the scaled average
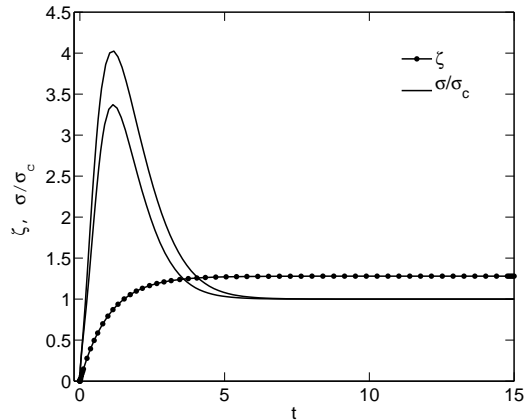
23

Figure 4.4: The time evolution of the the scaled average size ζ and the width σ/σ_c for different approximations of $\tilde{\Delta}'(\zeta)$. Compare with the corresponding PCM results in the inset of figure 4.3a. The time axis is relative.

size $\zeta(t) = \bar{x}/x_0$ and the scaled variance $\omega = \sigma^2/\sigma_c^2$ with respect to time:

$$\dot{\zeta} = (1 + |\bar{\mu}|) - \zeta \tag{4.3}$$
$$\dot{\omega} = 2 - 2\tilde{\Delta}'(\zeta)\,\omega \tag{4.4}$$

where $\tilde{\Delta}'(\zeta) = \Delta'(x)/\Delta'(x_c)$ and $\sigma_c^2 = 1/(\beta|\Delta'(x_c)|)$ is the width at the stationary position x_c. The solution of these equations is shown in figure 4.4. The results show that the stationary values of the mean and standard deviation are $1 + |\bar{\mu}|$ and σ_c, respectively, and the amount of overshooting is the skewness $|\bar{\mu}|$. The prediction of the time evolution made by the continuous model with stationary Gaussian distribution and linear drift velocity agrees well with numerical results.

4.3.2 Physical origin of overshooting

The origin of the overshooting is the drift velocity $v_{eff} \neq 0$ at free energy difference minimum, as described in reference [21] and Paper **IV**. The drift velocity $v_{eff}(\bar{x}) = d\bar{x}/dt$ arises from the difference of the chemical potential of certain nanodot Δ_{dot} and the average chemical potential $\bar{\Delta}$. One can find an approximative nanodot size corresponding to the average chemical potential. The nanodots for which $\Delta_{dot} > \bar{\Delta}$ tend to dissociate and the nanodots

with $\Delta_{dot} < \bar{\Delta}$ tend to grow. At the early stages of growth, the distribution is in the region of negative slope in chemical potential, $d\Delta/dx < 0$ and the nanodots are growing. The nanodots above the location of average chemical potential have a forward drift. Below the location of average chemical potential, the drift is negative and it pushes the tail of the distribution backwards to small sizes. The drift velocity enforces the distribution over the minimum of chemical potential to region $d\Delta/dx > 0$. The stationary size distribution observed in numerical solutions is found explicitly at this region of small positive gradient of chemical potential. Also the sharpening of the distribution occurs there.

The thermal diffusion tends to broaden the distribution stochastically. Diffusion is weak compared to the drift velocity at the fast growth stages. Only in stationary state, the drift velocity is low enough, such that the diffusion and drift can balance. Over the inflection point of chemical potential ($\Delta''(x_i) = 0$), the drift velocity is yet lower and diffusion causes inverse ripening of nanodots (see [22], figure 5.) In experimental situations, especially at low deposition fluxes, the distribution may never reach the inflection point, because of the long time scales and low drift velocities. The direct numerical integration solution of RKM [22] does not include realistic time scales and allows the distribution to develop over the inflection point $\Delta''(x) = 0$, unlike PCM simulation which, even with the event-based algorithm, cannot proceed over the stationary state in reasonable computing times. However, within MED scheme, the distribution cannot reach the thermodynamical stable state occuring at the minimum of total free energy, where $\Delta(x) = 0$. The nucleation theoretic calculation with Gibbs-Boltzmann equilibrium distribution [55] points out that the stable distribution ($dn/dt = 0$) settles in the total energy minimum (Appendix A of Paper **IV**).

4.3.3 Skewness-corrected distribution

The size distribution n_s at stationary size attains a nearly Gaussian form with small, but persistently remaining skewness, as found in Paper **II**. The skewness is connected to the drift velocity (Paper **II**, figure 9) and to the inflection point of the chemical potential and uniquely describes the growth stage of the distribution (Appendix A of Paper **IV**). However, it is not possible to calculate the numerical value of skewness within the continuous model, and therefore the numerical values are obtained from simulations. The effect of skewness is taken into account in the continuous model by including skew-

ness into the model of stationary distribution. The *skewed size distribution* n_x is assumed to be a Gaussian distribution with a linear skewness-dependent correction factor (Paper **IV**)

$$n = \left[1 + g_0 \left(\frac{x - \bar{x}}{\bar{x}}\right)\right] \frac{\exp\left[-(x - \bar{x})^2/2\delta^2\right]}{\sqrt{2\pi\delta^2}} \qquad (4.5)$$

where the scaled size is $x = s/s_0$ and dispersion (scaled width) is $\delta = w/\bar{s}$. The parameter g_0 is directly related to the skewness, $\mu_3 = 3g_0\delta$. The mean size of dots is then $\bar{x}$. The standard deviation of the distribution is temperature dependent, given by $w = 1/\sqrt{\beta|\Delta'(\bar{x})|}$ (Paper **II**).

5

Analytical prediction of selected size

5.1   Calculation

The analytical calculation to determine the selected size is done using the skewness-corrected RKM. The derivation is based on the equations (2.1)–(2.2).

In the study of Pirkkalainen et al. [22] the efficiency of the numerical solution of RKM is enhanced by stationarity approximations. The direct numerical solutions of rate equations are unnecessarily retarded by the extremely slow time evolution of adatom density at the early stages of growth, when dimers are formed. This bottleneck can be bypassed with two simplifying assumptions: stationarity of adatom density $dN_1/dt = 0$, and prevention of dimer formation from adatoms by setting $\sigma_1 = 0$ [22]. The approximate rate equations are

$$\frac{dn_2}{d\tau} \simeq -(N_1\sigma_2 + \gamma_2)n_2 + \gamma_3 n_3 \tag{5.1}$$

$$\frac{dn_s}{d\tau} = \sigma_{s-1}n_{s-1}N_1 - \sigma_s n_s N_1 + \gamma_{s+1}n_{s+1} - \gamma_s n_s \tag{5.2}$$

with $N_1 = n_1/\kappa$ and $\tau = \kappa t$. The stationary adatom density is now obtained: ($\Phi = \phi/\kappa$ is the scaled deposition flux)

$$N_1^{stat} = \frac{\Phi + \gamma_2 n_2 + \sum_{s\geq 2}\gamma_s n_s}{\sum_{s\geq 2}\sigma_s n_s}. \tag{5.3}$$

The practical starting point of the calculation is this equation (5.3). The notation $N_1 = N_1^{stat}$ is for simplicity. The assumption of stationarity removes all time dependencies of the size distribution. The approximation of insignificantly low dimer density in stationary state is made ($n_2 \approx 0$). The adatom flux is Φ, and the physical origin of the flux can be the molecular beam of adatoms filling the surface, or the flux of detached adatoms in the case of ion beam assisted deposition. Using detailed balance

$$N_1 = \frac{\Phi}{\sum_{s \geq 2} \sigma_s n_s} + \frac{\sum_{s \geq 2} \sigma_s e^{\beta \Delta} n_s}{\sum_{s \geq 2} \sigma_s n_s}. \tag{5.4}$$

In this calculation, the approximation $e^{\beta \Delta} \approx 1 + \beta \Delta$ is done and the free energy difference is expanded around the (yet unknown) mean of the size distribution $\bar{x} = \bar{s}/s_o$:

$$\Delta(x) \approx \Delta(\bar{x}) + \Delta'(\bar{x})(x - \bar{x}) + (1/2)\Delta''(\bar{x})(x - \bar{x})^2. \tag{5.5}$$

By performing the continuum limit calculation of equation (5.4) with attachment $\sigma_s \to x^q$ and the expanded free energy difference, the stationary adatom density is found:

$$N_1 = \frac{\Phi}{\bar{x}^q} + 1 + \beta \Delta(\bar{x}) + \frac{g_0 \beta \Delta'(\bar{x}) \delta^2}{\bar{x}} + \frac{1}{2} \beta \Delta''(\bar{x}) \delta^2. \tag{5.6}$$

At stationary state the quantity $\bar{\Delta}$, the average chemical potential of the size distribution, is defined:

$$N_1 = \frac{1}{\bar{x}^q} \int_{-\infty}^{\infty} x^q e^{\beta \Delta} n_x dx \equiv e^{\beta \bar{\Delta}} \iff \beta \bar{\Delta} = \ln N_1. \tag{5.7}$$

The drift velocity of the mean size is $v_{eff}(\bar{x}) = \bar{x}^q \beta[\bar{\Delta} - \Delta(\bar{x})]$ [21]. Drift is obtained by approximating $x \gg 1$ and using analytical prediction of width w, giving

$$v_{eff}(\bar{x}) = \Phi + \bar{x}^{q-1} \left[g_0 \, \text{sign}\,(\Delta'(\bar{x})) + \frac{\bar{x}}{2} \frac{\Delta''(\bar{x})}{|\Delta'(\bar{x})|} \right]. \tag{5.8}$$

The selected size $\bar{x}$ of the nanodot distribution at stationary state is obtained from the drift velocity of the distribution. After determining the size $\bar{x}$, one can define unitless *overshooting factors* $\bar{x}/x_0$, describing the amount by which the distribution exceeds the free energy difference minimum x_0. The overshooting factors are studied for two different growth situations; for the case of metal nanodots with more realistic energy function, and for the Ge/Si quantum dots in IBAD growth with phenomenological energy.

5.2 Metal nanodots

The size selection in growth of 2D metal nanodots (see reference [22]) is studied at stationary state in the absence of external flux ($\Phi = 0$). For free energy difference of metal dots the form introduced by Liu [43] is used:

$$\Delta(x) = -x^{-1}\log(ex) + 2\alpha e^{-\frac{1}{2}}x^{-\frac{1}{2}}, \qquad (5.9)$$

with x being the scaled dot size $x = s/s_0$, where s_0 is the dot size at the minimum of free energy difference. The first term of equation (5.9) is the contribution of edge energy and the second term is the surface energy of the dot. The parameter α is proportional to the nanodot substrate geometry and it is the relative strength of the edge energy to the surface energy. For details of the choice of parameters, see reference [22].

The numerical results of the 2D metal nanodot growth are presented in reference [22], and they are obtained by direct numerical integration of the growth equations (5.1)-(5.2). The analytical prediction of the selected size is calculated in Paper **IV**. The drift is vanishing at stationarity, and we obtain the equation for the distribution mean size $\bar{x}$:

$$\bar{x}\frac{\Delta''(\bar{x})}{\Delta'(\bar{x})} = g \qquad (5.10)$$

where parameter $g = -2g_0 = -2\mu_3/3\delta$. This equation defines implicitly the selected size $\bar{x}$.

The equation (5.8) is not defined at $\Delta'(x_0) = 0$. The points x_0, which are the free energy difference minima, are solved analytically using the Lambert W function [68] giving real and complex multivalued roots, of which the correct root is chosen (and shown in figure 5.1):

$$x_0 = \frac{4e}{\alpha^2}\left[W\left(-\frac{\alpha}{2\sqrt{e}}\right)\right]^2. \qquad (5.11)$$

The selected size $\bar{x}$ is analytically solved for potential (5.9) using equation (5.10). The solution is, with correct root of the Lambert W function (Paper **IV**)

$$\bar{x} = \frac{4e(2+g)^2}{\alpha^2(\frac{3}{2}+g)^2}\left[W\left(-\alpha\,\frac{\frac{3}{2}+g}{4+2g}\exp[-\frac{1+g}{4+2g}]\right)\right]^2. \qquad (5.12)$$
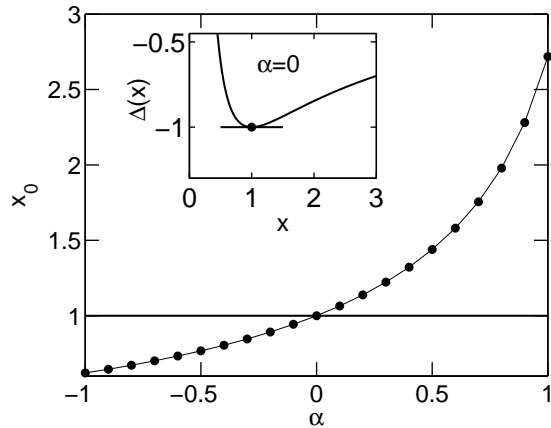
Figure 5.1: The zeros of the first derivative of free energy difference, $\Delta'(x_0) = 0$ as a function of the parameter α. The inset shows the minimum of the free energy difference Δ at $\alpha = 0$.

The results for the selected size $\bar{x}$ are obtained graphically from figure 5.2a as the intersection points of the derivative curves and the skewness parameter g. The MED data of direct numerical integration of RKM is presented by the solid dots ($\bullet$) and is seen to produce rather constant value of parameter g with region $-1 \leq \alpha \leq 0.5$. The constant value of g is thus justified. Four approximative levels of skewness, $g = 8, 5, 2$ and 0, are presented. The last value $g = 0$ corresponds to the total energy minimum (see Appendix A of Paper **IV**).

The overshooting factors $\bar{x}/x_0$ are in figure 5.2b. The distributions overshoot the free energy difference minimum by a factor 1.1–1.7 depending on the skewness. The overshooting, being independent of the preceding growth stages, enables fast deposition-driven preparation of the distribution to region $\bar{x}/x_0 \approx 1.5$, after which the self assembly stabilizes the distribution into its final sharp form. In concordance to this, the MED data of reference [22] with high deposition flux produces distributions with approximately zero skewness and a large overshooting factor.
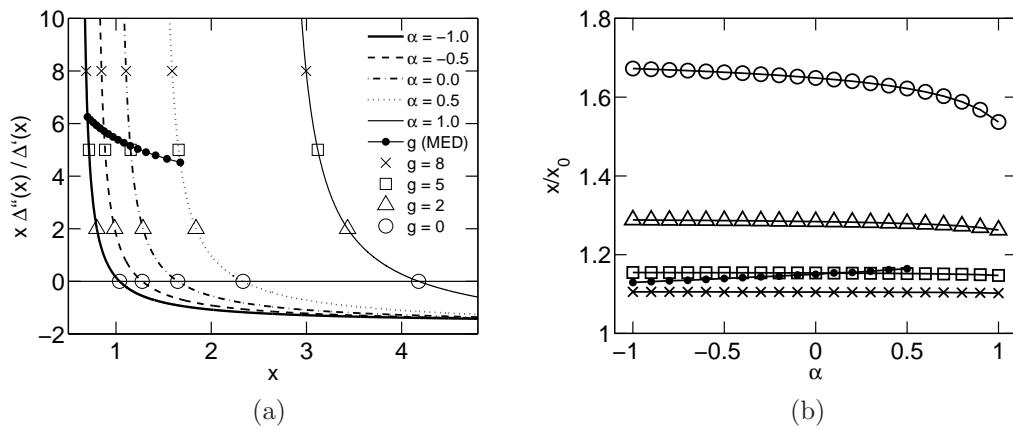
Figure 5.2: The data set "MED" (symbol ●) is the result of direct numerical integration of RKM as a function of α, and the data points are calculated from values of skewness μ_3 and dispersion δ of reference [22] with $g = -2\mu_3/3\delta$. From MED data is seen that the approximation $g = const.$ is rather good. Therefore, the constant values of parameter g are shown for four different values by symbols $\times$, $\square$, $\triangle$ and $\bigcirc$. Figure a): The solution of equation 5.10 presented graphically. The derivative curves, shown with solid and dashed lines, describe the left-hand side of equation 5.10 as a function of α. The solution $\bar{x}$ of equation 5.10 is read from the figure by finding the x-coordinate of the crossing point of the appropriate derivative curve and the (constant) level of parameter g. Figure b): The overshooting factors as a function of α with four different skewness values.

5.3 Semiconductor nanodots in ion beam assisted deposition

The growth of 3D semiconductor nanodots is studied experimentally in [23, 69], where the distributions of stationary Ge/Si nanodots are reported for molecule beam epitaxy (MBE) and ion beam assisted deposition (IBAD). The adatom flux of the growth system affects the size selection and it is different in MBE and IBAD. In conventional MBE growth, the flux $F = 0$ [50]. In *continuous* IBAD the ion beam generates a flux of adatoms, approximately corresponding to values $F \approx 0.01$ [23]. For *pulsed* IBAD the flux is much smaller, $0 < F \ll 0.01$, because the free surface adatoms recombine with surface defects between ion pulses. Therefore the flux needs to be taken into account in equation (5.8).

5.3.1 Double well energy

The thermodynamical energy of a growing nanodot in MBE or in IBAD alone is described through the phenomenological energy function. For free energy difference we use the form introduced by Gai et al. [42]:

$$\Delta(x) = w_0 + cx^\alpha + x^{-p}, \tag{5.13}$$

the details of which are explained in Section 3.2. The energy parameters c, α and p are related by the equation

$$s_0^{\alpha+p} = \frac{p}{\alpha c} \tag{5.14}$$

where s_0 is size corresponding to the minimum of the chemical potential.

The energy parameters c and α are different for MBE and IBAD. For conventional MBE, the heteroepitactic Ge/Si dots are strained and the strain exponent $\alpha_{MBE} = 1/3$. The minima of chemical potential are deduced from the mean of the measured size distribution of reference [23], giving approximately $s_{MBE} = 10^4$, corresponding to the value $c_{MBE} \approx 0.0022$. The main effect of IBAD is to reduce the nanodot self energy by facilitating the strain relaxation, thus lowering the strain exponent to value $\alpha_{IBAD} = 0.01$ and the chemical potential minimum to size $s_{IBAD} = 500$, corresponding to value $c_{IBAD} \approx 3.95$. In scaled variables $x_{IBAD} = 1$ and $x_{MBE} = 20$. Parameter p is chosen equal to the growth exponent, $p = q = 1/3$ for 3D dots.
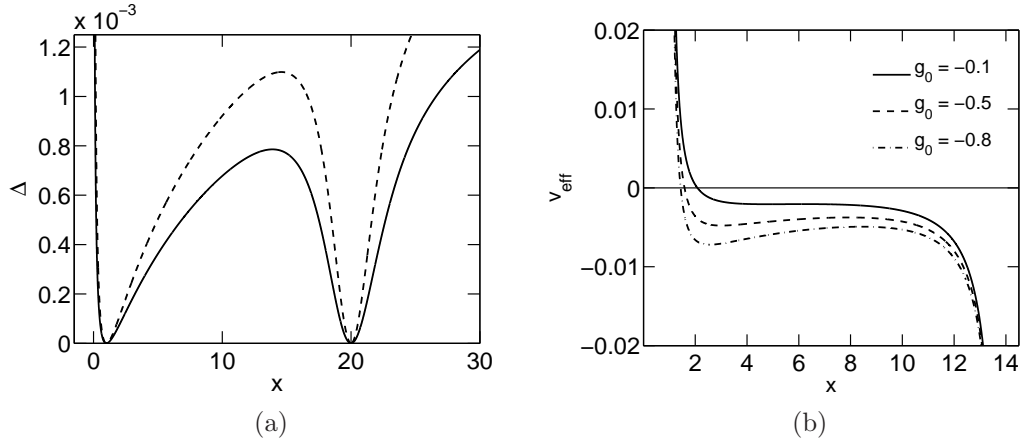
Figure 5.3: Figure a): The normalized total free energy difference Δ as a function of the scaled size x. The minima occur at sizes $x_0 = 1$ for IBAD and $x = 20$ for MBE. The energy function is shown for two values of exponent q: solid line corresponds to $q = 1/3$ and dashed line to $q = 1/2$. Figure b): The drift velocity (equation (5.8)) shown with three different skewness values, and without flux ($\Phi = 0$).

In growth occuring under MBE and IBAD together, the total energy function Δ is defined as a parallel operation of two growth modes:

$$\frac{1}{\Delta} = \frac{1}{\Delta_{MBE}} + \frac{1}{\Delta_{IBAD}} \tag{5.15}$$

with Δ_{MBE} and Δ_{IBAD} given above. The normalized double well energy $\Delta = w_0 + (1/\Delta_{MBE} + 1/\Delta_{IBAD})^{-1}$ with depth control parameter (having value $w_0 = 0$ for now) is shown in figure 5.3a.

5.3.2 Results of analytical model

The prediction of the selected size of nanodot distribution is calculated using the continuum model (Paper **V**). At stationary state the drift velocity disappears, giving from equation (5.8)

$$v_{eff}(\bar{x}) = \Phi + \bar{x}^{q-1} \left[g_0 \, \text{sign} \left(\Delta'(\bar{x}) \right) + \frac{\bar{x}}{2} \frac{\Delta''(\bar{x})}{|\Delta'(\bar{x})|} \right] = 0. \tag{5.16}$$
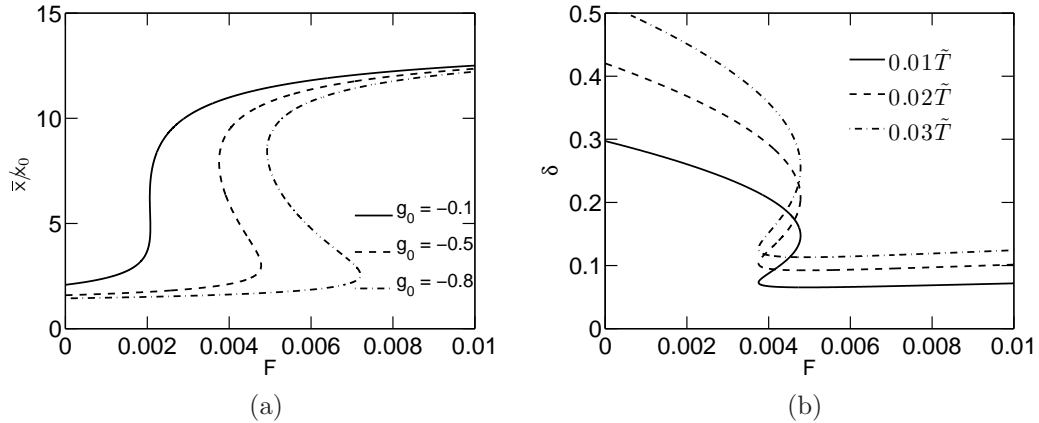
Figure 5.4: Figure a): The overshooting factors as a function of flux with three different skewness values g_0. Figure b): The dispersion δ as a function of the scaled temperature $\tilde{T}$. The skewness factor $g_0 = -0.5$.

The analytical solution of this equation is cumbersome; instead the numerical solution is preferable. The effective drift velocity of the first potential well without flux is in figure 5.3b. The negative drift velocity after the first minimum of thermodynamical energy at $x = 1$ pushes the distribution downwards to the spontaneously selected stationary state found in Paper **II**. However, the distribution can find a stationary form when an external flux $F \neq 0$ is applied. Stationarity occurs at any location of positive gradient of the energy below the saddle point of the potential (see figures 5.3a and 5.3b). At the vicinity of the saddle point the distribution broadens.

With fluxes $0.001 < F < 0.01$ the distribution is stationary and the mean size is shown in figure 5.4a. The overshooting factor at low fluxes is approximately $\bar{x}/x_0 \approx 2$, corresponding to the pulsed IBAD. The skewness g_0 affects the stationary size by enhancing the drift towards smaller sizes (Figs. 5.3b and 5.4a). For larger skewness values, a larger external flux F is needed to obtain the stationary distribution.

The optimum distribution is found when the dispersion δ of the distribution is the smallest (figure 5.4b). The optimum at $\delta = 0.1$ is found above the spontaneously selected state, and with the external flux $F \approx 0.004$. At this point the increasing of the ion bombardment flux F does not improve the size selection further, but enlarges the dispersion. At the limit of continuous

IBAD, the dispersion increases steadily, corresponding to saddle point region, where $x/x_0 \approx 12 - 15$. The corresponding temperature region is $0.01 < \tilde{T} < 0.03$.

The results are in agreement with experimental results [23], where the ratio $x_c/x_p = (L_c/L_p)^3 \approx 21$, where x_p and x_c are the stationary sizes, and L_p and L_c are the nanodot base lengths for pulsed and continuous IBAD, respectively. The dispersion of the pulsed IBAD distribution is $\delta_p \approx 0.25$, in agreement with the prediction of the stationary region $\bar{x} \approx 2x_0$ (see figure 5.4b). The dispersion of the continuous IBAD distribution is $\delta_c \approx 0.75$, but the experimental data is not of Gaussian type, but rather a bimodal distribution, and the standard deviation is not obtained accurately. The model predicts, however, the sharpening of the distribution at fluxes $F \approx 0.004$.

5.3.3   Results of nucleation theoretic approach

Ultimately, the ion bombardment of nanodots leads to formation of bimodal distributions, when part of the distribution exceeds the saddle point of thermodynamical energy and further proceeds towards the stationary location of the other potential well. Bimodal distributions are studied in Appendix B of Paper **V** using the nucleation theoretic approach [55]. The basic assumptions behind the nucleation theory are the presence of continuous monomer source, or dilute dot system to quarantee the adequate amount of adatoms surrounding the nucleating dots, and the "vapour-independent" break-up (detachment) of dots. In RKM the detachment rate only depends on the size of the dot. The total mass conservation in nucleation theoretic calculation is not assumed, unlike in RKM.

The stable size distribution is obtained, when $dn(s)/dt = 0$ for every size s. The nucleation current J through the system is found and the detailed balance is broken. (In equilibrium the current $J_e = 0$, and total mass conservation and detailed balance are valid.) The stable current is (see reference [55], p. 91)

$$J = \left[\sum_{s=1}^{\infty} \left(\frac{1}{\sigma_s n^e(s) S^s} \right) \right]^{-1} \tag{5.17}$$

where σ_s is the attachment rate, and the factor $n^e(s) S^s$ is the saturation-corrected equilibrium distribution,
$n^e(s) S^s = \exp(-\Delta W_s/kT)$. The reversible work ΔW_s of forming a cluster of
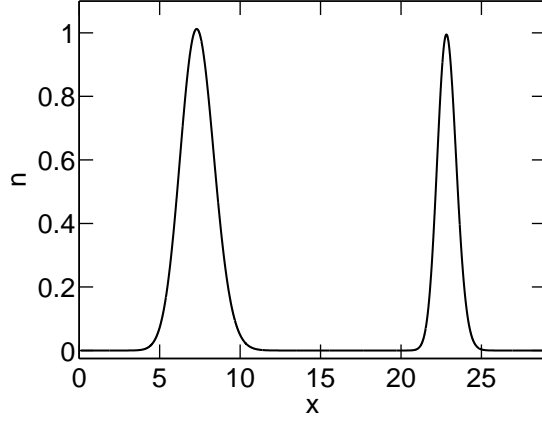
Figure 5.5: The stable bimodal distribution obtained with nucleation theoretic calculation. The n-axis is in relative units. The mean sizes of the distributions occur at $\bar{x}_1 = 7.3$ and $\bar{x}_2 = 22.8$. The dispersions $\delta = w/\bar{s}$ are $\delta_1 = 0.143$ and $\delta_2 = 0.026$. The temperature $T = 400$K.

size s is [70]

$$\Delta W_s = -kT \sum_{j=2}^{s} \ln\left(\frac{\sigma_{j-1}}{\gamma_j}\right). \tag{5.18}$$

The stable densities (or concentrations) can be shown to be [55]

$$n(s) = \exp\left(\frac{-\Delta W_s}{kT}\right) \left[1 - \frac{\sum_{i=1}^{s-1}\left(\sigma_i \exp(-\frac{\Delta W_i}{kT})\right)^{-1}}{\sum_{j=1}^{\infty}\left(\sigma_j \exp(-\frac{\Delta W_j}{kT})\right)^{-1}}\right] \tag{5.19}$$

The distribution $n(s)$ is calculated with double well thermodynamical energy Δ. The summation to infinity in equation (5.19) is in practice a summation to large enough size index N_0, at which the distribution becomes independent of the value of the index. Note, that the reversible work ΔW_s is different from the energy Δ, and the energy Δ is included into the rates σ and γ in equation (3.1). Example of the stable distribution is in figure 5.5. The depth w_0 of the potential Δ adjusts the selected size by acting as an effective external flux. When the potential is lower, the relative mass of the second peak grows driven by the kinetics caused by the effective flux.

The mean $\bar{x}$, standard deviation w and skewness μ_3 are determined individually for both of the peaks of the stable distributions. The mean sizes of

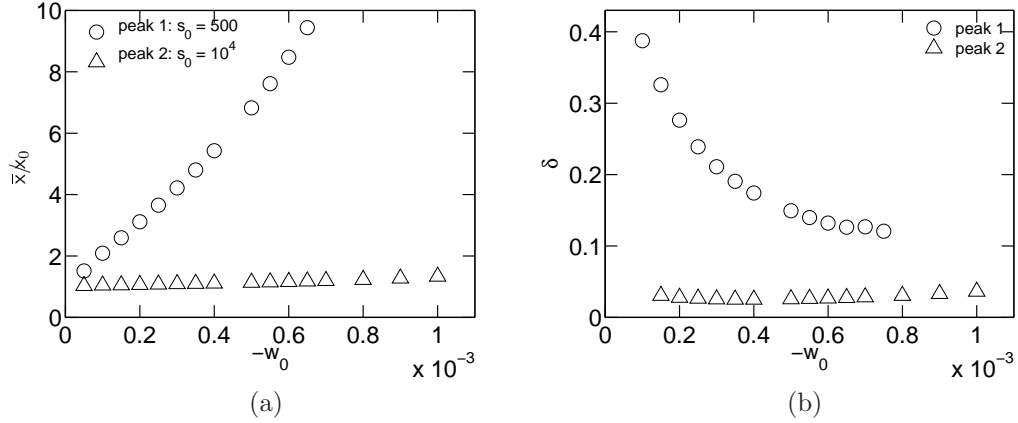(a)   (b)

Figure 5.6: Figure a): The overshooting factors for stable bimodal distribution as a function of the potential depth w_0. The mean sizes of the peaks are shown individually. Temperature is $T = 400K$. Compare the data shown with circles ($\bigcirc$) with figure 5.4a. Figure b): The dispersion of each peak of stable bimodal distribution as a function of the potential depth w_0. Temperature is $T = 400K$. Compare the data shown with circles ($\bigcirc$) with figure 5.4b.
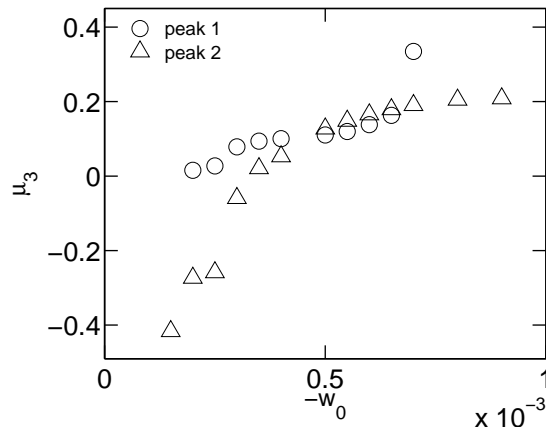

Figure 5.7: The skewness for each peak of stable bimodal distribution as a function of the potential depth w_0. Temperature is $T = 400K$. The skewness of the first peak (circles $\bigcirc$) is approximately constant.

both peaks shift as a function of the potential depth w_0, as shown in figure 5.6a. The dispersion $\delta = w/\bar{s}_0$ and skewness are in figures 5.6b and 5.7. It is curious to observe, that the stable state results of mean and dispersion are qualitatively very similar to the continuum model predictions at stationary state in figures 5.4a and 5.4b. The stable value of skewness in first peak is $\mu_3 \approx 0.1$. From this fact is interpreted that the stable distribution has exceeded the inflection point of the energy before the saddle point (see Paper **IV**, Appendix A). However, the skewness can be approximated constant in the first peak by using data of figure 5.7 and thus the constant value of skewness in the stationary state result is justified (figure 5.4a).

The results of this chapter show that the continuous growth model can be used to predict quantitatively the selected size in nanodot growth systems. The stationary state results of the continuous model are in qualitative agreement with the stable results obtained by using the nucleation-theoretic approach.

6

Summary

In this thesis the object was to study the self-organized growth of nanodots by numerical simulations and mesoscopic reaction kinetic based modelling. A continuous model, derived from the reaction kinetics, was utilized to clarify the features of reversible nanodot growth under kinetic and thermodynamical energy contributions. The experimental size selection of nanodots is a detailed process, and control of the selected size and the shape of the dot distribution is desirable. This work provides methods to predict and adjust the optimal mean size and sharpness of the nanodot size distributions.

The power-law type kinetic growth, present at various contexts in nature, was studied in a strongly reversible adatom aggregate system by stochastic simulation of the reaction kinetic model. Different growth and decay exponents were studied, and the scaling of the size distributions was found. The values of scaling exponents and the scaling function were determined. The numerical results were in accordance with scaling theory predictions of power-law growth, and the results of the continuous growth model. (Paper **I**)

The self assembled growth in heteroepitaxial nanodot systems was considered by including the thermodynamical energy within the model by a self consistent rate scheme. The stochastic numerical simulations of Monte Carlo type with event-based algorithm were used to enlighten the time development of the size distribution. Three stages of growth were found: at the beginning the early, singular growth similar to the power-law growth, secondly the short-lived metastable state of kinetic origin, and thirdly the stationary state formed by the interplay of the kinetics and the thermodynamical energy. The size selection with narrow size distribution occurs at the stationary

state. The overshooting phenomenon at stationary state was observed: the mean size exceeds notably the minimum of the free energy difference. The accurate shape of the size distribution was clarified to be a skewed Gaussian. (Paper **II**)

The other, independent numerical scheme was used to calculate the size distributions. The direct numerical integration of rate equations, according to the master equation discretization scheme, provides similar results for the time development and stationary state size distribution. This guarantees that the solution of the reaction kinetic model is correct, and both the stochastic simulation and the direct numerical integration schemes can equivalently be used to solve the growth problem. (Paper **III**)

The continuous model was used to reproduce the numerical data. The Fokker-Planck type growth model, derived by assuming the Gibbs-Boltzmann equilibrium distribution and the validity of the detailed balance of transitions, predicts the time evolution of the distribution with respect to the stationary state. The overshooting is described only qualitatively, when the skewness, which cannot be currently determined within the continuous model, acts as an external parameter and its values are obtained from numerical simulations. (Papers **II** and **III**)

The effort to quantitatively predict the stationary size and overshooting from the continuous model was made. It turns out, that the expression for drift velocity of the size distribution can be derived analytically by assuming constant adatom density at stationary state. The results of the overshooting were found to be in agreement with numerics. (Paper **IV**) Finally, the analytical prediction of the selected size was tested against experimental Ge/Si nanodot growth data with agreement (Paper **V**). The nucleation theoretic calculations, related closely to the growth model, provide the details of the stable distributions, toward which the stationary distribution is proceeding extremely slowly (Papers **IV** and **V**).

This thesis shows that the simple continuous growth model can be used to describe the size selection in nanodot growth. The numerical simulations and the model results are quantitatively in good agreement. The thermodynamical potentials of this study have been phenomenological, and the results are thus at general level, but with more detailed potentials the model would be able to realistically describe certain experimental situations. An open question is, if a reasonably complicated evaluation of the skewness is possible within the continuous model.

Appendix A: Errata of Paper II

The equation (3), which is equal to the equation (A.3), should read

$$
\begin{aligned}
\sigma_s &= s^q/(\xi + e^{\beta \Delta_s}) \\
\gamma_s &= s^q/(1 + \xi e^{-\beta \Delta_{s-1}})
\end{aligned}
$$

where the parameter ξ is the correlation length and its value in simulations is $\xi = 0.01$.

Appendix B: Errata of Paper III

The equations (4) and (5) should read

$$\begin{aligned}
\sigma_s &= s^q/(\xi + e^{\beta \Delta_s}) \\
\gamma_s &= s^q/(1 + \xi e^{-\beta \Delta_{s-1}})
\end{aligned}$$

where the parameter ξ is the correlation length and its value is $\xi = 0.01$. The equation (8) should read

$$\frac{dn_s}{dt} = D_-[D_-(\kappa \gamma_{s+1} n_{s+1})] - D_-[(n_1 \sigma_s - \gamma_s) n_s].$$

Bibliography

[1] J. Blum, G. Wurm, S. Kempf, T. Poppe, H. Klahr, T. Kozasa, M. Rott, T. Henning, J. Dorschner, R. Schrpler, H. U. Keller, W. J. Markiewicz, I. Mann, B. A. S. Gustafson, F. Giovane, D. Neuhaus, H. Fechtig, E. Grn, B. Feuerbacher, H. Kochan, L. Ratke, A. El Goresy, G. Morfill, S. J. Weidenschilling, G. Schwehm, K. Metzler and W.-H. Ip, Phys. Rev. Lett. **85**, 2426 (2000).

[2] M. Krause and J. Blum, Phys. Rev. Lett. **93**, 021103 (2004).

[3] J. Xin, S. Wang, Y. Wang J. Yuan, W. Zhang, Y. Sung, Atmospheric Environment **39**, 5971 (2005).

[4] T. Cheng, D. Lu, H. Chen, Y. Xu, Atmospheric Environment **39**, 1237 (2005).

[5] K. Park, Y. Lai, Y. Nong, Phys. Rev. E **72**, 026131 (2005).

[6] S. V. Buldyrev, N. V. Dokholyan, S. Erramili, M. Hong, J. Y. Kim, G. Malescio, H.E. Stanley, Physica A **330**, 653 (2003).

[7] J. Laherrére, D. Sornette, Eur. Phys. J. B **2**, 525 (1998).

[8] T.Michely, J.Krug: *Islands, Mounds and Atoms*, Springer, Heidelberg (2004).

[9] K. Pirkkalainen, K. Leppänen, U. Vainio, M.A. Webb, T. Elbra, T. Kohout, A. Nykänen, J. Ruokolainen, N. Kotelnikova and R. Serimaa, Eur. Phys. J. D **49**, 333 (2008).

[10] D.J. Norris, Al. L. Efros, M. Rosen, and M. G. Bawendi, Phys. Rev. B **53**, R16347 (1996).

[11] M.S. Skolnick and D.J. Mowbray, Ann. Rev. of Material Res. **34**, 181 (2004).

[12] B. Zorman, M. V. Ramakrishna and R. A. Friesner, J. Phys. Chem. **99**, 7649 (1995).

[13] P.B. Joyce, T. J. Krzyzewski, G. R. Bell, and T. S. Jones, S. Malik, D. Childs, and R. Murray, Phys. Rev. B **62**, 10891 (2000).

[14] F. Rosei, J. Phys. Condens. Matter **16**, S1373 (2004).

[15] F. Patella, A. Sgarlata, F. Arciprete, S. Nufris, P.D. Szkutnik, E. Placidi, M. Fanfoni, N. Motta, and A. Balzaroti, J. Phys. Condens. Matter **16**, S1503 (2004).

[16] E.H.C. Parker (Ed.): *The Technology and Physics of Molecular Beam Epitaxy*, Plenum Press, New York (1985).

[17] B. Degroote, A. Vantomme, H. Pattyn and K. Vanormelingen, Phys. Rev. B **65**, 195401 (2002).

[18] H.T. Dobbs, D.D. Vvedensky, A. Zangwill, J. Johansson, N. Carlsson, and W. Seifert, Phys. Rev. Lett. **79**, 897 (1997).

[19] H.M. Koduvely, and A. Zangwill, Phys. Rev. B **60**, R2204 (1999).

[20] G.S. Bales and A. Zangwill, Phys. Rev. B **55**, R1973 (1997).

[21] T.P. Munt, D.E. Jesson, V.A. Shchukin, and D. Bimberg, Phys. Rev. B **75**, 085422 (2007).

[22] K. Pirkkalainen, and I.T. Koponen, Surf. Sci. **604**, 951 (2010).

[23] A.V. Dvurechenskii, J.V. Smagina, R. Groetzschel, V.A. Zinovyev, V.A. Armbrister, P.L. Novikov, S.A. Teys, and A.K. Gutakovskii, Surf. Coat. Tech. **196**, 25 (2005).

[24] F. Leyvraz, Phys. Rep. **383**, 95 (2003).

[25] P. Bak, C. Tang, K. Wiesenfeld, Phys. Rev. Lett. **59**, 381 (1987).

[26] J. A. Blackman and A. Marshall, J. Phys. A: Math. Gen. **27**, 725 (1994).

[27] J. R. King and A. D. Wattis, J. Phys. A: Math. Gen. **35**, 1357 (2002).

[28] J.A.D Wattis and P. V. Coveney, J. Phys. A: Math. Gen. **34** 8679 (2001).

[29] M. Rusanen, I.T. Koponen and J. Asikainen, Eur. Phys. J. B **36**, 567 (2003).

[30] I.T. Koponen, M.O. Jahma, M. Rusanen and T. Ala-Nissilä, Phys. Rev. Lett. **92**, 086103 (2004).

[31] R. Becker and W. Döring, Ann. Phys **4**, 719 (1935).

[32] J. J. L. Velázquez, J. Stat. Phys. **92**, 195 (1998).

[33] H. Risken, *The Fokker-Planck Equation*, Springer, Berlin (1984).

[34] K. S. Fa and E. K. Lenzi, Phys. Rev. E **67**, 061105 (2003).

[35] N. Metropolis and S. Ulam, Journal of the American Statistical Association **44**, 335 (1949).

[36] K. Kang and S. Redner, Phys. Rev. A **30**, 2833 (1984).

[37] K. Kang, S. Redner, P. Meakin and F. Leyvraz, Phys. Rev. A **33**, 1171 (1986).

[38] P.L. Krapivsky, J.F.F. Mendes, S. Redner, Eur. Phys. J. B **4**, 401 (1998).

[39] F. Liu, A.H. Li, and M.G. Lagally, Phys. Rev. Lett. **87**, 126103 (2001).

[40] M. Kobayashi, T.M. Ramachandran, P. Chen, and A. Madhukar, Appl. Phys. Lett. **68**, 3299 (1996).

[41] D. Leonard, and K. Pond, and P.M. Petroff, Phys. Rev. B **50**, 11687 (1994).

[42] Z. Gai, B. Wu, G.A. Farnan, D. Shu, M. Wang, Z. Zhang and J. Shen, Phys. Rev. Lett. **89**, 235502 (2002).

[43] F. Liu, Phys. Rev. Lett. **89**, 246105 (2002).

[44] J. Shen, J.P. Pierce, E.W. Plummer and J. Kirschner, J. Phys. Condens. Matter **15**, R1 (2003).

[45] F. Komori, S. Ohno and K. Nakatsuji, J. Phys. Condens. Matter **14**, 8177 (2002).

[46] D.J. Eaglesham, and M. Cerullo, Phys. Rev. Lett. **64**, 1943 (1990).

[47] C. Priester, and M. Lannoo, Phys. Rev. Lett. **75**, 93 (1995).

[48] M. Meixner, E. Schöll, V.A. Shchukin and D. Bimberg, Phys. Rev. Lett. **87**, 236101 (2001).

[49] M. Meixner, R. Kunert and E. Schöll, Phys. Rev. B **67**, 195301 (2003).

[50] D.E. Jesson, T.P. Munt, V.A. Shchukin, and D. Bimberg, Phys. Rev. Lett. **92**, 115503 (2004).

[51] V.A. Shchukin, and D. Bimberg, Rev. Mod. Phys. **71**, 1125 (1999).

[52] R.E. Rudd, G.A.D. Briggs, A.P. Sutton, G. Medeiros-Ribeiro, and R.S. Williams, Phys. Rev. Lett. **90**, 146101 (2003).

[53] D. Kashchiev, Cryst. Res. Technol. **19**, 1413 (1984).

[54] D. Kashchiev, *Nucleation: Basic Theory with Applications*, Butterworth-Heinemann, Oxford (2000).

[55] H. Vehkamäki, *Classical Nucleation Theory in Multicomponent Systems*, Springer, Berlin Heidelberg (2006).

[56] J. Tersoff and R.M. Tromp, Phys. Rev. Lett. **70**, 2782 (1993); F.M. Ross, J. Tersoff and R.M. Tromp, Phys. Rev. Lett. **80**, 984 (1998).

[57] R. Bahadur and R. B. McClurg, J. Chem. Phys. **121**, 12499 (2004).

[58] A. Lo and R. T. Skodje, J. Chem. Phys. **112**, 1966 (2000).

[59] A.B. Bortz, M.H. Kalos, J.L. Lebowitz, J. Comp. Phys. **17**, 10 (1975).

[60] D.R. Cox and H.D. Miller, *The Theory of Stochastic Processes*, Methuen, London (1965).

[61] W.M. Young and E.W. Elcock, Proc. Phys. Soc. **89**, 735 (1966).

[62] J. Heinonen, Ph.D. thesis, Aalto University, 2001, http://lib.tkk.fi/Diss/2001/isbn9512252864/

[63] R. Grima, T.J. Newman, Phys. Rev. E **70**, 036703 (2004).

[64] R. Metzler, Eur. Phys. J. B **19**, 249 (2001).

[65] F. Benamira, and L. Guechi, Europhys. Lett. **56**, 8 (2001).

[66] C.F. Lo, Europhys. Lett. **39**, (1997) 263; P. Demo, A.M. Sveshnikov, Z. Kožíšek, Europhys. Lett. **50**, 278 (2000).

[67] J.C. Neu, L.L. Bonilla, A. Carpio, Phys. Rev. E **71**, 021601 (2005).

[68] R. Corless, G. Gonnet, D. Hare, D. Jeffrey, D. Knuth, Adv. Comp. Mat. **5**, 329 (1996).

[69] A.V. Dvurechenskii, V.A. Zinovyev, and Zh.V. Smagina, JETP Lett. **74**, 296 (2001).

[70] J. Merikanto, H. Vehkamäki, and E. Zapadinsky, J. Chem. Phys. **121**, 914 (2004).